

# The Use of Landsat 8 in Detecting Potential Mineral Zones in West Nusa Tenggara, Indonesia

Umar A. Said<sup>1</sup>, Rashad A. Bantan<sup>1</sup> (<https://orcid.org/0000-0002-0226-0418>), Ammar A. Manaa<sup>1</sup> (<https://orcid.org/0000-0002-1857-4171>), Yasser Taufiq<sup>2</sup>

<sup>1</sup>Marine Geology Department, King AbdulAziz University. Jeddah, Saudi Arabia

<sup>2</sup>PT. Sumbawa Timur Mining, Jakarta, Indonesia

\* **Correspondence to:** Umar Abdulrahim Said, [usaid@stu.kau.edu.sa](mailto:usaid@stu.kau.edu.sa)

Received: DATE 2024.

Accepted

Published:

© 2024. The Authors.

**Abstract:** The remote sensing analysis within the Hu'u District area is known to face a challenge with dense vegetation. The problem affects the accurate reading of spectral reflectance from satellites, influencing the differentiation between potential mineral zones and vegetation. Therefore, this study aims to carry out a remote sensing analysis of densely vegetated areas to differentiate minerals from vegetation and obtain potential mineral zones. The combination band ratios and principal component analysis (PCA) methods are used to acquire potential mineral zones. Furthermore, Landsat 8 images freely available on Google Earth Engine are adopted and the validation is carried out using a drill hole from previous study. The results show that band ratios method cannot distinguish mineral zones from vegetation. However, PCA method can recognize potential mineral zones. This is the result from PCA method with band combination of bands 1, 2, 3, 4, 5, and 6 as the first group and bands 2, 4, 5, and 6 as the second group.

**Keywords:** Landsat 8, Band Ratio, Principal Component Analysis, Mineral, Densely Vegetated



---

## 1. Introduction

Geological mapping is perceived as an indispensable component across different disciplines and applications. In this context, remote sensing datasets have been developed as a cost-effective, efficacious, as well as temporally and labor-efficient methodology, particularly when subjected to traditional approaches of field mapping. Landsat data has also been extensively deployed for tasks such as discriminating among rock units, deciphering lineaments, and showing hydrothermal alterations. Due to economic concerns, mineral mapping using satellite data speeds up exploration, lowers expenses, as well as accurately and quickly identifies broad regions (Aita and Omar, 2021; Bakardjiev and Popov, 2015; Naftali et al., 2015; Shebl and Csamer, 2021).

Optical appraisal of aerial pictures has been leveraged to correctly show these formations, particularly linear structures or lineaments. In the present era, with the advent of Geographic Information System (GIS) expertise, the high-resolution data gained from photos, autonomous parsing of satellite images, and Landsat, is strongly propagated (Wambo et al., 2016). Alteration mineral indices such as the OH-bearing, pyrophyllite, kaolinite, alunite, and calcite were established by detecting argillic, phyllic, and propylitic alternations in epithermal deposit and porphyry copper deposit using Landsat 8 (Ombiro et al., 2021; Parcutela et al., 2022; Shim et al., 2021; Zhang et al., 2016).

Several studies have focused on methodologies to show geological structures by taking advantage of Principal Component Analysis (PCA) and Band Ratio (BR) among other techniques. The use of the conventional PCA approach may substantially enhance the precision of geological mapping, facilitating a more accurate identification and interpretation of geospatial and spectral data (Carranza and Hale, 2010; Chen et al., 2021; Ghasemi et al., 2018).

## 2. Study Area

The study area is located within the Hu'u district, Dompu Regency on Sumbawa Island, situated in West Nusa Tenggara, Indonesia, and forms a portion of the territory under projects managed by PT Sumbawa Timur Mining (PT STM). Within the district, there exist three principal porphyry Cu-Au prospects, specifically the Humpa Leu East, Sori Hiu, and Onto prospects (Fadlin et al., 2023). The district has been hypothesized to be a paleovolcano, characterized by Upper Miocene Basaltic Andesite lava, with radiometric dating at an age of  $5 \pm 0.2$  Ma years. Regionally, the rock formations are categorized as constituents of the Old Volcanics Rocks Formation (Verdiansyah et al., 2023). The Hu'u intricate features various surface possibilities, manifested as a lithocap of widespread epithermal-style alteration but some are connected to a porphyry situated underneath the ground (Verdiansyah et al., 2021).

The Hu'u project region is situated at the junction of many significant fault zones, according to a seismotectonic assessment. A significant sinistral fault with an NW trend is projected across the region from the southwest face of the Tambora volcano. Furthermore, a significant dextral fault with an NE trend extends along the bay straight west of the Hu'u region (Burrows et al., 2020).

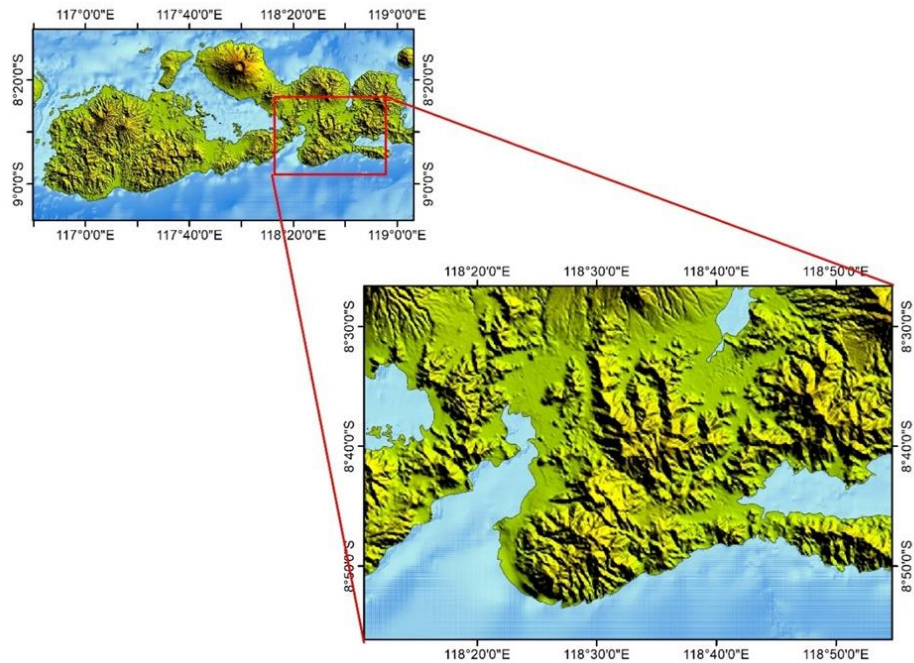


**Figure 1.** Hu'u District, West Nusa Tenggara, Indonesia as the study area

### 3. Method

#### 3.1 Images Data

Landsat 8 data used is freely obtained from Google Earth Engine as a compilation of images from April 2013 to 2023. This data is pre-configured in a Top of Atmosphere (TOA) format after radiometric and geometric corrections. Furthermore, cloud cover filter is the preprocessing conducted to obtain the least cloudy images. The purpose of the pre-processing is to derive a collection of satellite images, spanning several years, with minimal cloud interference.

#### 3.2 Pre-Processing

The data, procured from the Google Earth Engine, originates from Landsat 8, Collection 2, Tier 1. This data is pre-configured in a TOA format after radiometric and geometric corrections. In addition, the pre-processing is to derive a collection of satellite images, spanning several years, with minimal cloud interference. Obtaining raw Landsat satellite images in the region of interest is crucial in providing the conditions in the targeted area.

#### 3.3 Band Ratio

Band combinations tested in this study are 4/2, 6/7, 6/5, and 7/5 to obtain iron oxide, hydroxyl-bearing rocks, ferrous minerals, and clay, respectively.

#### 3.4 Band Ratio Composites

The 3 combinations of band ratio composites experienced in the project are Sabin's ratio, Kaufmann's ratio, and composite of 4/2, 6/7, and 5. Sabin's ratio is expected to define a hydrothermal alteration map, while Kaufmann's ratio is anticipated to distinguish altered rocks and lithological elements from the vegetation.

The composites of 4/2, 6/7, and 5 are used to differentiate altered rocks and outcrops from trees and plants.

### 3.5 PCA

There are two combinations of bands for PCA. The group of bands 1, 2, 3, 4, 5, and 6, as well as those from bands 2, 4, 5 and 6. Eigenvalue and eigenvector are required to calculate visualization in RGB format.

## 4. Results

### 4.1 Raw Landsat Satellite Images

The true color composite requires the visual combinations of bands 2, 3, and 4 from Landsat 8 satellite. The image area should have a low cover of clouds to disturb the reflectance of signal from a satellite. The cloud covering is inversely proportional to the accuracy of the results. From Figure 2, the region of interest can be known as a densely vegetated area, disturbing the reflectance of signal from a satellite. Meanwhile, the signal reads the vegetation instead of mineral and an advanced analysis is essential to obtain the reflection of mineral under tight vegetation. Figure 2 is a compilation of Landsat 8 images from April 2013 to 2023 freely available and obtained from Google Earth Engine showing true color composite.

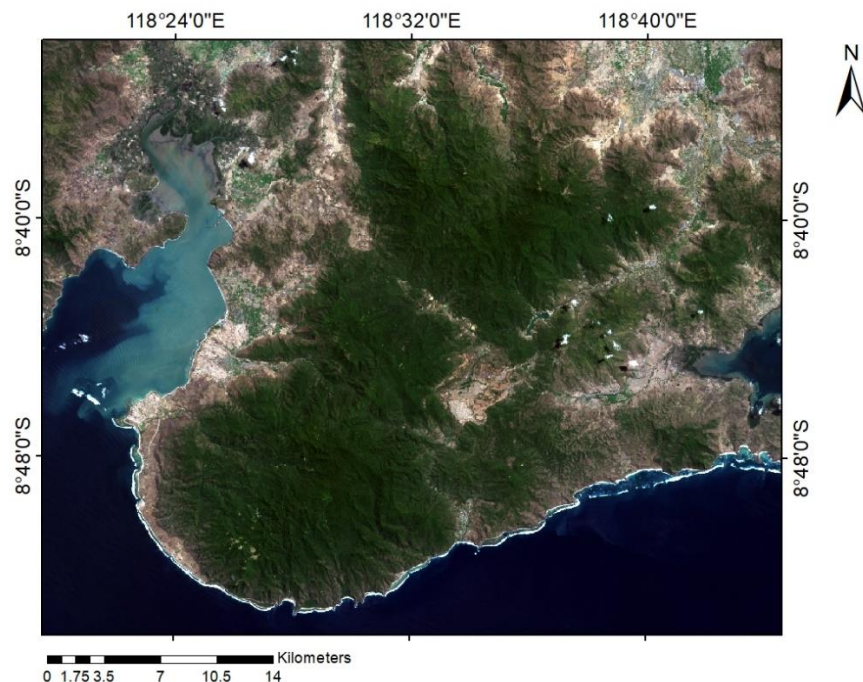


**Figure 2.** True color composites are presented by bands 2, 3, and 4 to explain the real condition of the study area with the least clouds.

### 4.2 Band Ratios

Figure 3A, 3B, 3C, and 3D shows the results of band 4/2, 6/7, 6/5, and 7/5, respectively. Mineral potential zone is not reported due to vegetation and the expected result is unachieved by combining some bands. Therefore, this method does not apply to the study area due to increased vegetation.

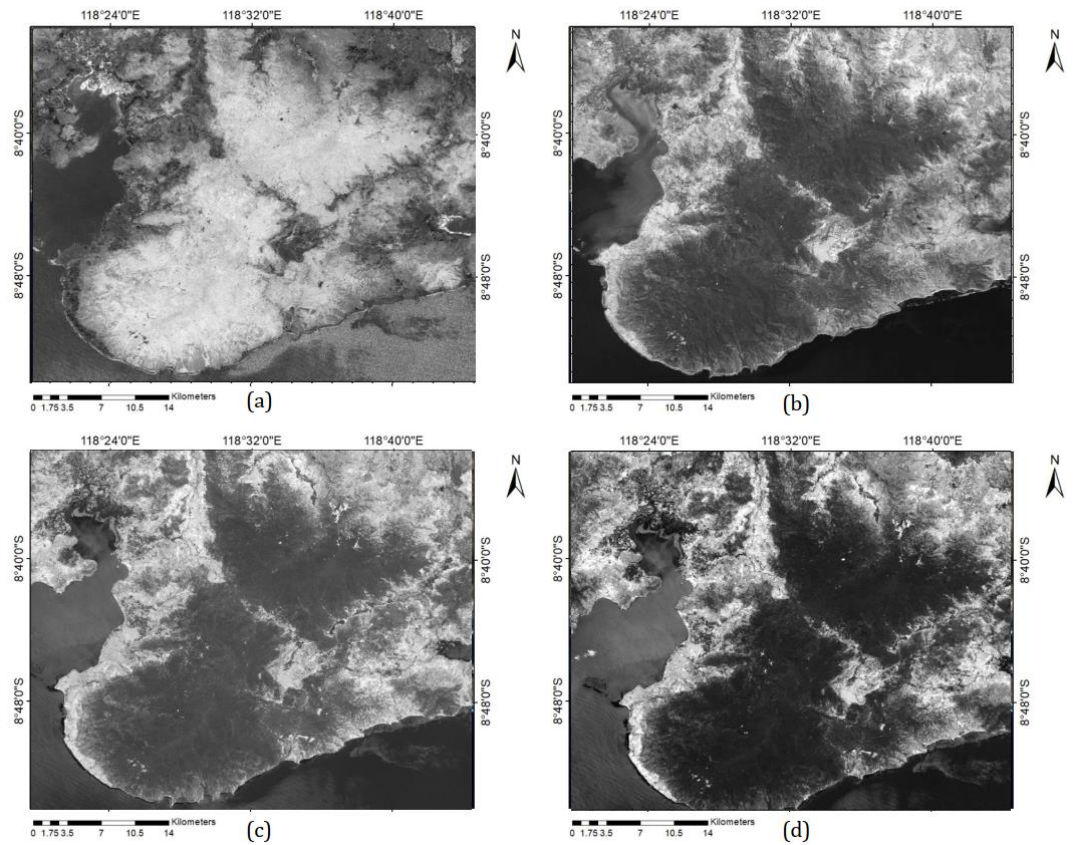


**Figure 3.** (a) Band ratio 4/2, (b) Band Ratio 6/7, (c) Band Ratio 6/5, (d) Band Ratio 7/5. These combinations were conducted to detect potential zones.

### 4.3 Band Ratio Composites

Sabin's ratio is expected to define the hydrothermal alteration map by combining bands 4/2, 6/7, and 6/5. Kaufmanns' ratio is anticipated to distinguish altered rocks and lithological units from the flora using a combination of 7/5, 5/4, and 6/7. Meanwhile, composites of 4/2, 6/7, and 5 are optimized to differentiate altered rocks and outcrops from woodlands. Figures 4A, 4B and 4C present the result of Sabin's ratio, Kaufmann's ratio, and a composite of 4/2, 6/7, and 5. These three composites cannot identify potential mineral zones and the vegetation is still the unworked factor. Even though the three bands are tested in one composite of RGB format, the expected result is not attained.

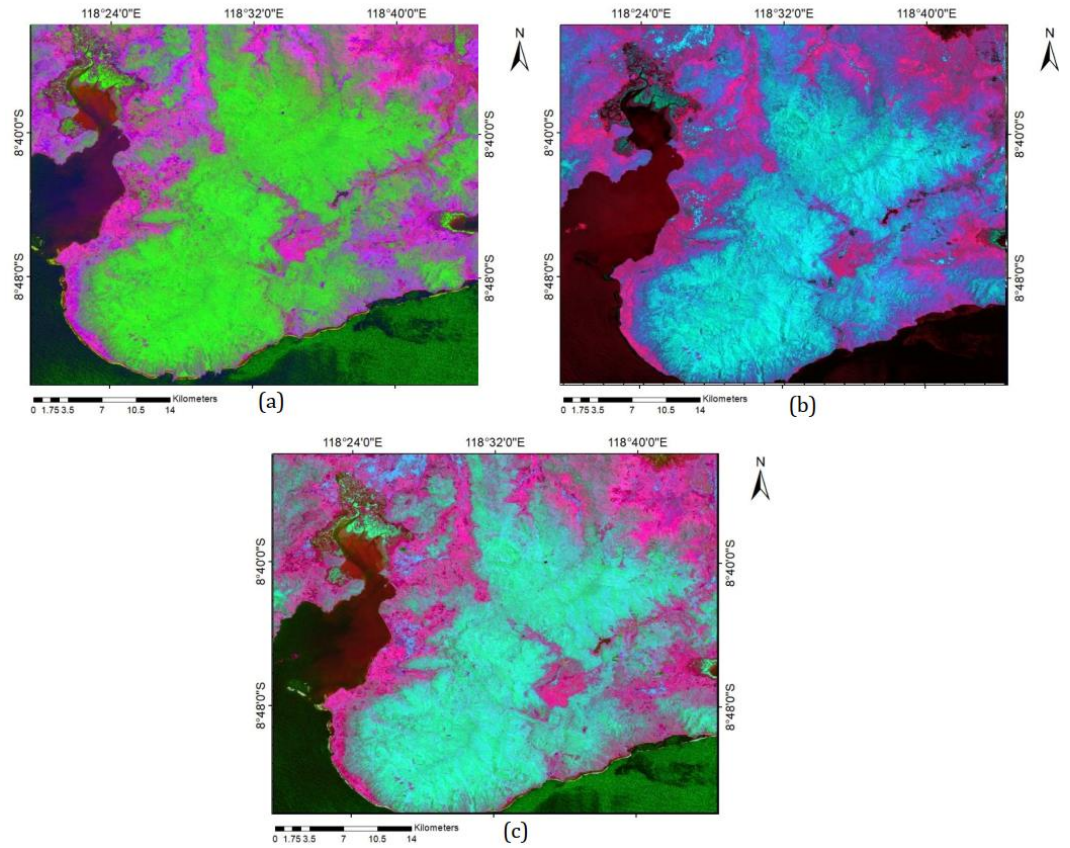


**Figure 4.** A) Sabin's Ratio (band 4/2, 6/7, and 6/5), B) Kaufmann's Ratio (band 7/5, 5/4, 6/7), C) Composite of 4/2, 6/7, 5

#### 4.4 PCA

The first combination group consists of bands 1, 2, 3, 4, 5, and 6 to recognize hydrothermally altered rocks and other minerals from trees. In addition, the second group of bands 2, 4, 5, and 6 are processed to obtain iron oxides from plants.

**Table 1.** Eigen Values and Eigen Vectors for Bands 1, 2, 3, 4, 5 and 6

	PC1	PC2	PC3	PC4	PC5	PC6
Band 1	0.020360	0.192974	-0.334840	-0.494944	0.402861	0.665554
Band 2	0.035911	0.238785	-0.402445	-0.452621	0.201009	-0.731068
Band 3	0.103666	0.253710	-0.484258	-0.032229	0.816609	0.149964
Band 4	0.155918	0.433000	-0.377308	0.723144	0.350531	0.005456
Band 5	0.754882	-0.595431	-0.265794	0.023034	0.066237	-0.007135
Band 6	0.627209	0.547126	0.527643	-0.160181	0.056473	0.002697
Eigen Values	0.026078	0.004487	0.001089	0.000040	0.000011	0.000001
Percentage of Eigen Values	82.251%	14.151%	3.436%	0.126%	0.035%	0.002%

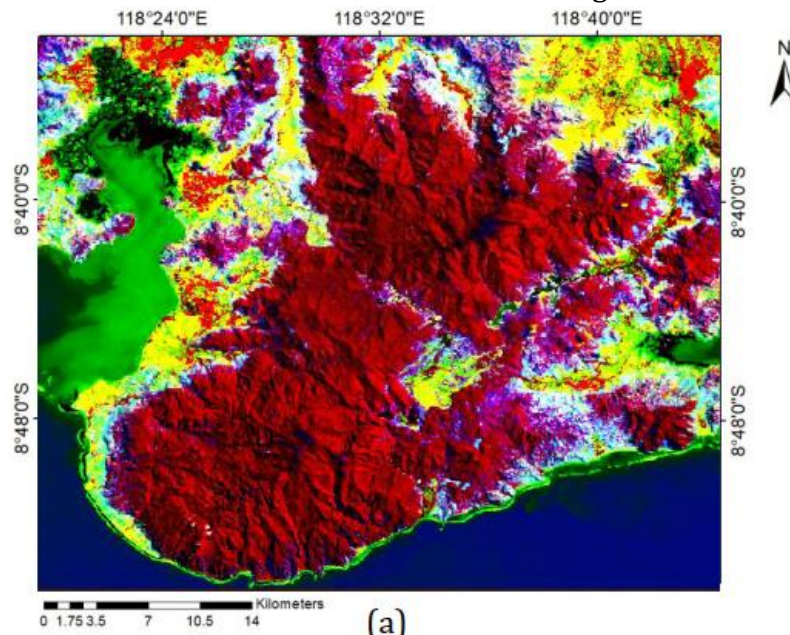
Cumulative Percentage of Eigen Values	82.251%	96.402%	99.837%	99.963%	99.998%	100.000%
---------------------------------------	---------	---------	---------	---------	---------	----------

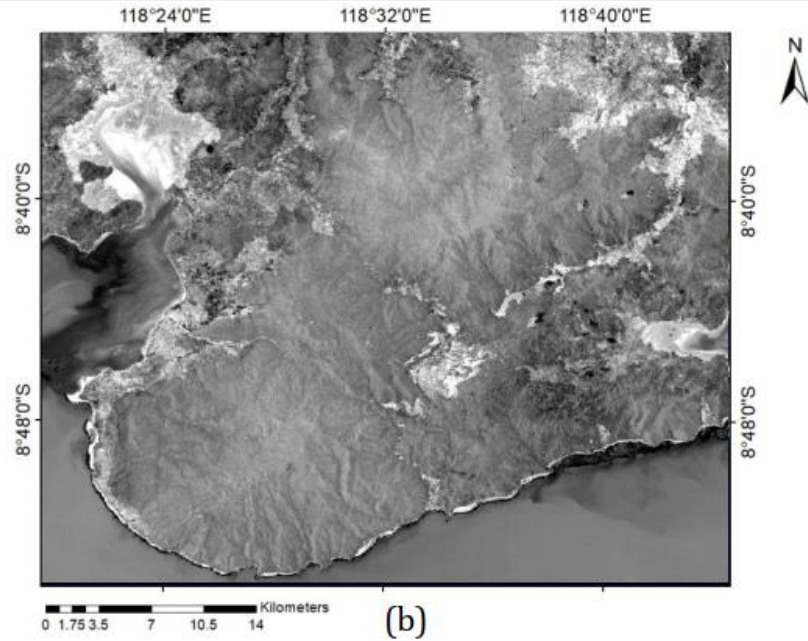
Table 1 shows that PC1, PC2, and PC3 account for 99.83% of the variation to create the RGB composite for producing the primary component seen in Figure 5A. According to the illustration, the green and blue colors symbolize flora and rocks subjected to hydrothermal alteration, respectively.

**Table 2.** Eigen Values and Eigen Vectors for Bands 2, 4, 5, and 6

	PC1	PC2	PC3	PC4
Band 2	-0.033644	0.223736	0.583605	0.779882
Band 4	-0.153175	0.432613	0.643692	-0.612408
Band 5	-0.761896	-0.611333	0.213294	-0.017100
Band 6	-0.628427	0.623747	-0.446734	0.128249
Eigen Values	0.025795	0.004078	0.000661	0.000027
Percentage of Eigen Values	84.40%	13.35%	2.16%	0.09%
Cumulative Percentage of Eigen Values	84.40%	97.75%	99.91%	100.00%

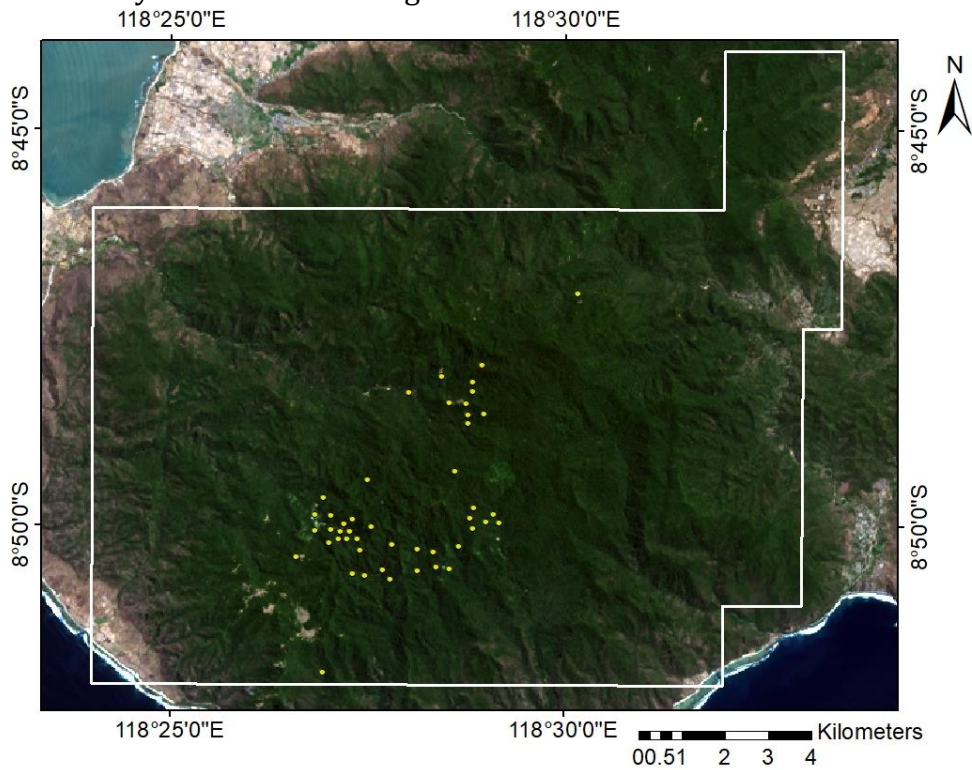
PC4 comprises 0.09% of the variance data and has the greatest loading positive and negative Eigenvector values of 0.779882 and -0.612408 for bands 2 and 4, respectively. In broad terms, minerals related to iron oxides show low absorption and reflectance between 0.64-0.67  $\mu\text{m}$  and 0.45-0.51  $\mu\text{m}$ , respectively. Therefore, regions connected to iron oxides in bands 2 and 4 are bright in the PC4 picture.





151  
152 **Figure 5.** A) The PC1, PC2, and PC3 components in RGB combination. Potential  
153 mineral zones are illustrated in dark blue. B) Principal component 4 (PC4). The bright  
154 pixels correspond to hydrothermally altered rocks.

155  
156 Figure 5A explains that potential mineral zones are depicted in dark blue, while  
157 vegetation is shown in green. In this context, the bright pixels represent  
158 hydrothermally altered rocks in Figure 5B.

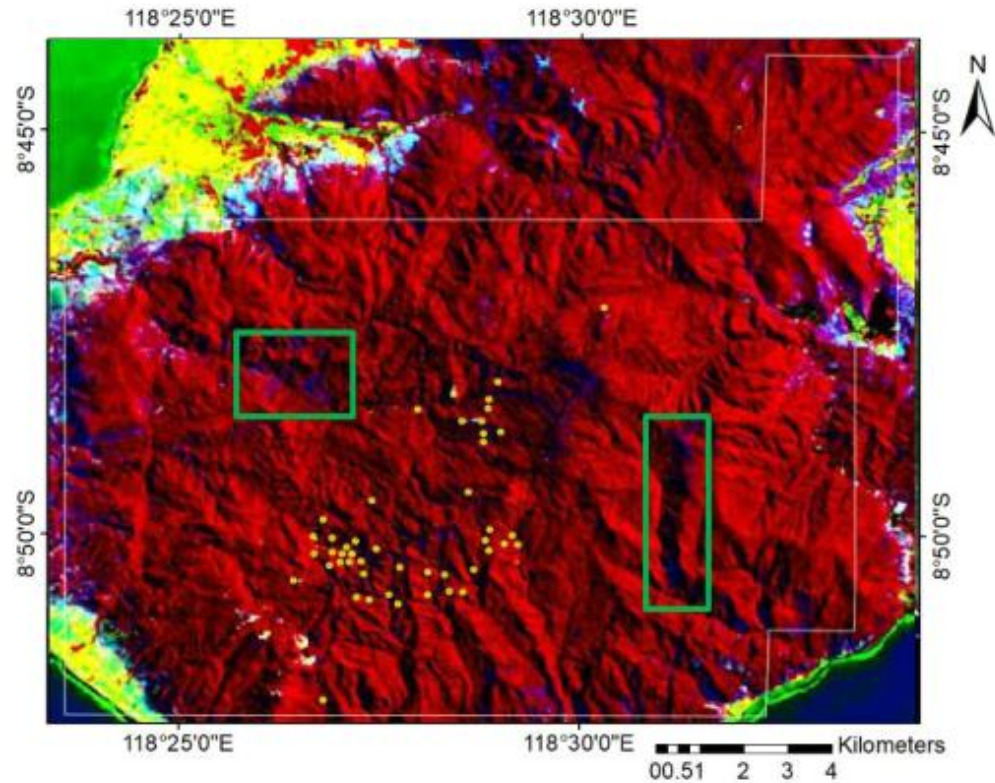


159  
160 **Figure 6.** Drill hole locations (modified after (Burrows et al., 2020)). The yellow  
161 dots and white lines are drill holes and project boundaries, respectively.

162  
163 The drill hole data and boundaries of the company's project area used are  
164 presented in Figure 6. The white lines and yellow dots represent the project area



165 boundaries and drill hole locations, respectively. From Figure 7, the locations of the  
166 drill holes are matched with the blue areas from the analysis representing potential  
167 mineral zones. Therefore, the green squares can be potential areas for upcoming  
168 exploration projects.



169 **Figure 7.** Validated map. Yellow dots are drill holes. Dark blue are potential  
170 mineral zone. The green boxes are the suggested next exploration areas.  
171

## 172 5. Discussion and Conclusion

173 The true color composite was reported to require the visual combinations of  
174 bands 2, 3, and 4 from Landsat 8 satellite. The image area had a low cover of clouds  
175 to disturb the reflectance of the signal from a satellite. The clouds covering was  
176 inversely proportional to the accuracy of the results and the region of interest could  
177 be known as a densely vegetated area. In this context, the vegetation disturbed the  
178 reflectance of the signal from a satellite. Therefore, an advanced analysis is essential  
179 to obtain the reflection of minerals under tight vegetation.

180 Band ratios 4/2, 6/7, 6/5, and 7/5 were tested as visualized in Figure 3 but  
181 could not differentiate mineral potential zone. The vegetation disturbed the satellite  
182 signal reflectance and the expected result could not be accomplished by combining  
183 some bands. Therefore, this method did not apply to this study area due to high  
184 vegetation. Sabin's Ratio (band 4/2, 6/7, and 6/5), Kaufmann's Ratio (band 7/5, 5/4,  
185 6/7), and composite of band 4/2, 6/7, 5 were also examined as shown in Figure 4.

186 Advanced analysis was conducted using PCA and potential mineral zones were  
187 visible. Based on eigenvalue and eigenvector calculations, PC1, PC2, and PC3  
188 possessed data variance of more than 99.83% in RGB format. The dark blue and green  
189 tint sections showed possible mineral zones and flora, respectively. Meanwhile, the  
190 bright pixels represented hydrothermally altered rocks in Figure 5B. Figure 7 shows

---

191 that mineral zones from PCA method were located as drill holes and yellow dots were  
192 drill holes from the previous study. Dark blue zones were potential mineral areas and  
193 the green boxes were the suggested exploration areas.

194 In conclusion, PCA method could reduce the effect and identify the targeted  
195 zones even though the vegetation disturbed the read of the satellite signal in detecting  
196 mineral areas. The integration of the method with machine learning might produce  
197 clearer differences for potential zones.  
198

## 199 References

- 200 Aita, S. K., and Omar, A. E. (2021): Exploration of uranium and mineral deposits using remote sensing  
201 data and GIS applications, Serbal area, Southwestern Sinai, Egypt, *Arabian Journal of Geosciences*, 1–  
202 17. <https://doi.org/10.1007/s12517-021-08568-0>
- 203 Bakardjiev, D., and Popov, K. (2015): ASTER spectral band ratios for detection of hydrothermal  
204 alterations and ore deposits in the Panagyurishte Ore Region, Central Srednogie, Bulgaria, **76**,  
205 79–88.
- 206 Burrows, D. R., Rennison, M., Burt, D., and Davies, R. (2020): The Onto Cu-Au Discovery, Eastern  
207 Sumbawa, Indonesia: A Large, Middle Pleistocene Lithocap-Hosted High-Sulfidation Covellite-  
208 Pyrite Porphyry Deposit, *Economic Geology*, **115**(7), 1385–1412.  
209 <https://doi.org/10.5382/econgeo.4766>
- 210 Carranza, E. J. M., and Hale, M. (2010): Mineral imaging with Landsat Thematic Mapper data for  
211 hydrothermal alteration mapping in heavily vegetated terrane, **1161**.  
212 <https://doi.org/10.1080/01431160110115014>
- 213 Chen, Q., Zhao, Z., Zhou, J., Zeng, M., Xia, J., Sun, T., and Zhao, X. (2021): New Insights into the Pulang  
214 Porphyry Copper Deposit in Southwest China : Indication of Alteration Minerals Detected Using  
215 ASTER and WorldView-3 Data.
- 216 Fadlin, Takahashi, R., Agangi, A., Sato, H., Idrus, A., Sutopo, B., and Pratiwinda, R. (2023): Geology,  
217 mineralization and calcite-rich potassic alteration at the Humpa Leu East ( HLE ) porphyry Cu-Au  
218 prospect, Hu ' u district, Sumbawa Island, Indonesia, *Resource Geology*, **73**(October 2022), 1–32.  
219 <https://doi.org/10.1111/rge.12309>
- 220 Ghasemi, K., Pradhan, B., and Jena, R. (2018): Spatial Identification of Key Alteration Minerals Using  
221 ASTER and Landsat 8 Data in a Heavily Vegetated Tropical Area, *Journal of the Indian Society of*  
222 *Remote Sensing*, **46**(7), 1061–1073. <https://doi.org/10.1007/s12524-018-0776-0>
- 223 Naftali, A., Hede, H., Kashiwaya, K., Koike, K., and Sakurai, S. (2015): A new vegetation index for  
224 detecting vegetation anomalies due to mineral deposits with application to a tropical forest area,  
225 1–50.
- 226 Ombiro, S. O., Olatunji, A. S., Mathu, E., and Ajayi, T. R. (2021): Application of remote sensing in mapping  
227 hydrothermally altered zones in a highly vegetative area - A case study of Lolgorien, Narok County,  
228 Kenya, *Indian Journal of Science and Technology*, (September).
- 229 Parcutela, N. E., Dimalanta, C. , Armada, L. T., Austria, R. S., Gabo-Ratio, J. A., and Jr., G. P. Y. (2022): Band  
230 processing of Landsat 8-OLI multi-spectral images as a tool for delineating alteration zones  
231 associated with porphyry prospects : A case from Band processing of Landsat 8-OLI multi-spectral  
232 images as a tool for delineating alteration zones associated, *IOP Conference Series: Earth and*  
233 *Environmental Science*, **1071**(012022). <https://doi.org/10.1088/1755-1315/1071/1/012022>

- 234 Shebl, A., and Cramer, A. (2021): Lithological , structural and hydrothermal alteration mapping utilizing  
235 remote sensing datasets : a case study around Um Salim area , Egypt Lithological , structural and  
236 hydrothermal alteration mapping utilizing remote sensing datasets : a case study arou.  
237 <https://doi.org/10.1088/1755-1315/942/1/012032>
- 238 Shim, K., Yu, J., Wang, L., Lee, S., Koh, S. M., and Lee, B. H. (2021): Content Controlled Spectral Indices for  
239 Detection of Hydrothermal Alteration Minerals Based on Machine Learning and Lasso-Logistic  
240 Regression Analysis, *IEEE Journal of Selected Topics in Applied Earth Observations and Remote*  
241 *Sensing*, **14**, 7435–7447. <https://doi.org/10.1109/JSTARS.2021.3095926>
- 242 Verdiansyah, O., Idrus, A., Setijadji, L. D., Sutopo, B., and Sukadana, I. G. (2021): Mineralogy of  
243 hydrothermal breccia cement of Humpa Leu East porphyry copper-gold prospect , Sumbawa Island  
244 , Indonesia, **04008**, 0–5.
- 245 Verdiansyah, O., Idrus, A., Setijadji, L. D., Sutopo, B., and Sukadana, I. G. S. (2023): Elemental mapping  
246 and mineral distribution of the Humpa Leu East porphyry samples: An implication to understand  
247 the pattern of mineralization, (June). <https://doi.org/10.1063/5.0126120>
- 248 Wambo, J. D. T., Ganno, S., Ngambu, A. A., Negue, E. N., Ondo, J. M., and Nzenti, J. P. (2016): Use of  
249 Landsat 7 ETM + Data for the Geological Structure Interpretation : Case Study of the Ngoura-  
250 Colomines Area , Eastern Cameroon, *Journal of Geosciences and Geomatics*, **4**(3), 61–72.  
251 <https://doi.org/10.12691/jgg-4-3-3>
- 252 Zhang, T., Yi, G., Li, H., Wang, Z., Tang, J., Zhong, K., Li, Y., Wang, Q., and Bie, X. (2016): Integrating Data of  
253 ASTER and Landsat-8 OLI ( AO ) for Hydrothermal Alteration Mineral Mapping in Duolong  
254 Porphyry Cu-Au Deposit , Tibetan Plateau, China, *Remote*, **8**(890).  
255 <https://doi.org/10.3390/rs8110890>
- 256
- 257